

K418 与 42CrMo 异种金属激光深熔焊接

庞 铭, 郑彩云, 刘秀波, 虞 钢

(中国科学院力学研究所, 北京 100080)

摘 要: 研究了连续波 Nd: YAG 激光焊接功率、速度、离焦量和侧吹保护气流量对激光深熔焊接 K418 与 42CrMo 异种金属焊缝形貌、焊缝熔深的影响, 讨论了焊缝区热裂纹产生机制。结果表明, 额定功率为 3 kW 的 Nd: YAG 激光深熔焊接 K418 与 42CrMo 异种金属, 由于它们的物理化学性质的差异, 焊缝靠近 42CrMo 侧易出现未熔合; 激光光斑向 42CrMo 侧偏移可以减少焊缝靠近 42CrMo 侧未熔合量; 通过优化侧吹保护气流量和离焦量可以增加熔深。由于 K418 液态金属的流动性差, 导致焊缝靠近 K418 侧对流传热不充分, 使焊缝靠近 K418 侧熔合线呈现锯齿形。焊缝区热裂纹的产生主要是由于焊缝区元素偏析形成的低熔物导致。

关键词: 激光焊接; 深熔焊; 焊缝; 热裂纹

中图分类号: TG456.7 文献标识码: A 文章编号: 0253-360X(2007)09-083-04



庞 铭

0 序 言

涡轮增压器转子的焊接是发动机制造的一项关键技术, 而涡轮增压器转子一般是由镍基铸造高温合金 K418 涡轮盘和合金调质钢 42CrMo 涡轮轴焊接而成, 二者的热物理性能、高温力学性能差异很大, 属于典型的异种金属的焊接^[1]。目前对这两种金属的焊接方法有电子束焊接和摩擦焊焊接。电子束焊接需要真空室和产生 X 射线, 而摩擦焊焊接常在熔合线附近发现缺陷, 合格率较低^[2]。由于目前焊接方法的不足, 中国科学院力学研究所激光智能制造与工艺力学试验室采用额定功率为 3 kW 的 Nd: YAG 固体激光器焊接这两种异种金属。

文中考察了激光焊接工艺参数(激光功率 P 、激光焊接速度 v 、离焦量 Δz 、侧吹保护气流量 q)对焊缝形貌、焊缝熔深 D_b 的影响, 并分析了焊缝区域热裂纹产生机制及硬度分布, 为激光焊接 K418 与 42CrMo 异种金属的生产应用提供参考。

1 试验材料和方法

材料为镍基铸造高温合金 K418 和合金调质钢 42CrMo, 厚度 7 mm, 其化学成分见表 1, 表 2。试验设备采用了 Nd: YAG 固体激光器, 额定输出功率 3 kW, 光束模式多模。聚焦镜镜头焦距 200 mm, 激

光从焦点半径 R 到光斑半径变为 $\sqrt{2}R$ 的距离为 1.6 mm (瑞利长度), 激光在瑞利长度范围内近似平行^[3]。侧吹保护气体为高纯度的氩气, 侧吹保护气角度 35° , 侧吹保护气吹气方向和焊接方向相反。K418 与 42CrMo 采用对接, 连续激光焊接, 中间不留间隙, 焊前用丙酮对试样清洗。激光焊接对工作台的精度要求很高, 试验通过千分表调整工作台的水平和垂直精度, 使其误差范围在 0.04 mm 内。焊后切取焊缝横截面, 抛光后用王水腐蚀焊缝和 K418, 用硝酸酒精腐蚀 42CrMo, 用光学显微镜及扫描电镜观察焊缝组织并测量焊缝熔深, 用能谱仪分析焊缝区域成分, 用硬度仪测量焊缝区域硬度。文中的焊缝熔深是指焊缝横截面 K418 与 42CrMo 都熔合上的深度。

2 结果分析

2.1 焊缝形貌

图 1 是在其它焊接参数相同的条件下, 改变激光光斑的偏移量, 图 1a 激光光斑在接头中心, 图 1b 42CrMo 侧占激光光斑 2/3。在图 1 中焊缝左边是 42CrMo, 右边是 K418。从图 1a 可以看出焊缝靠近 42CrMo 侧出现了未熔合, 这是由于 42CrMo 的热扩散率比 K418 高, 在 42CrMo 侧散失的热量多, 熔化 42CrMo 母材所需的能量临界值比 K418 侧高。K418 与 42CrMo 热物性参数见文献[4, 5]。当作用在焊缝处的能量介于 K418 与 42CrMo 熔化临界值时, 焊缝

表 1 K418 的化学成分(质量分数, %)

Table 1 Chemical composition of K418

C	Cr	Mo	Nb	Al	Ti	Zr	B
0.08~0.16	11.5~13.5	3.8~4.8	1.8~2.5	5.5~6.4	0.5~1.0	0.06~0.15	0.008~0.020
Mn	Si	P	S	Fe	Pb	Bi	Ni
≤0.50	≤0.50	≤0.015	≤0.010	≤1.0	≤0.001	0.0001	余量

表 2 42CrMo 的化学成分(质量分数, %)

Table 2 Chemical composition of 42CrMo

C	Cr	Mo	Mn	Si	P	S	Fe
0.38~0.45	0.90~1.20	0.15~0.25	0.50~0.80	0.20~0.40	≤0.040	≤0.040	余量

就发生偏移。对比图 1a, b 可以看出激光光斑偏向 42CrMo 侧可增加焊缝熔深和减少焊缝下侧的未熔合量, 这是由于激光光斑偏向 42CrMo, 增加了 42CrMo 侧的热输入值。

2.3 焊接速度的影响

图 3 是激光功率 3 kW, 离焦量 -1 mm, 侧吹保护气流量 15 L/min。可以看出, 焊缝熔深随激光焊接速度的增加而减少。速度对熔深的影响是由于随激光焊接速度的增加, 作用在焊缝处的激光焊接热输入减少。

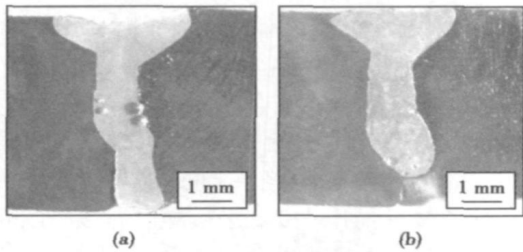


图 1 焊缝截面
Fig. 1 Cross section of weld

2.2 激光功率的影响

图 2 是激光焊接速度 15 mm/s, 离焦量 -1 mm, 侧吹保护气流量 15 L/min。可以看出, 焊缝熔深随激光功率的增加而增大。激光功率对熔深的影响是由于激光功率的增加, 增加了激光作用在焊缝处的能量。

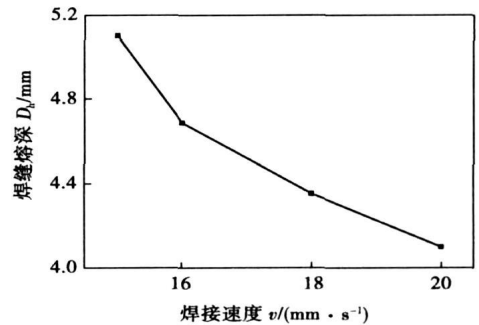


图 3 速度与焊缝熔深的关系
Fig. 3 Influence of welding velocity on weld depth

2.4 离焦量的影响

图 4 是激光功率 3 kW、速度 10 mm/s、侧吹保护气流量 5 L/min。定义焦平面在工件表面, 离焦量为 0; 可以看出, 焊缝熔深随离焦量的增加而先增大后减小。

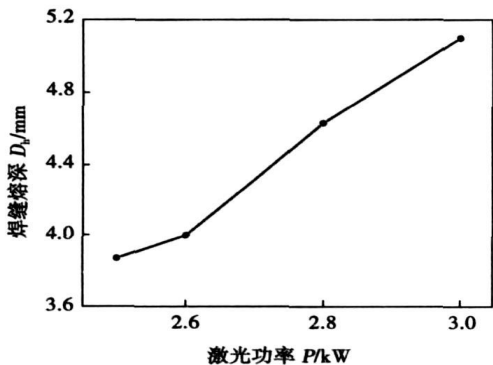


图 2 功率与焊缝熔深的关系
Fig. 2 Influence of laser power on weld depth

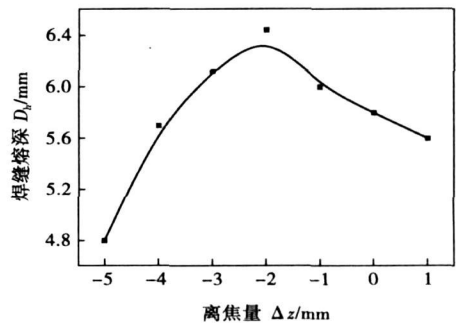


图 4 离焦量与焊缝熔深的关系
Fig. 4 Influence of defocusing distance on weld depth

焦平面在工件内部, 离焦量为负。从图 4 可以看出离焦量从 1 mm 变到 -2 mm, 熔深增加; 从 -2 mm 变到 -5 mm, 熔深减少。离焦量对熔深的影响是由激光束的传输特性决定的。

2.5 侧吹保护气流量的影响

图 5 是激光功率 3 kW, 速度 10 mm/s, 离焦量 0。激光焊接侧吹保护气作用是吹散焊缝正面的等离子云, 减少等离子云对激光的吸收、散射和折射^[6, 7]。从图 5 可以看出, 有一个临界侧吹保护气流量使焊缝熔深达到最大。侧吹保护气流量对焊缝熔深的影响是由侧吹保护气减少焊缝正面的等离子云及侧吹保护气流量的变化对深熔焊接熔池和匙孔稳定性的影响的综合作用。

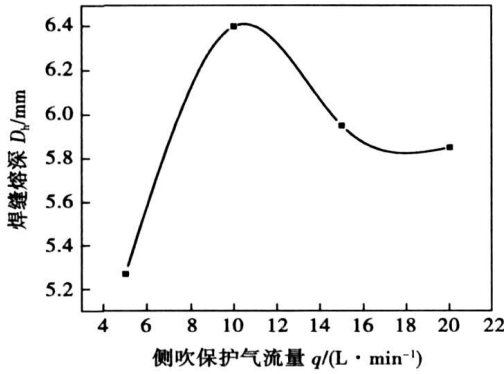


图 5 侧吹保护气流量对焊缝熔深的影响

Fig. 5 Influence of side-blow shielding gas flow rate on weld depth

3 焊接接头组织与力学性能

从图 6 可以看出焊缝区硬度介于母材 K418 与 42CrMo 硬度之间, 42CrMo 侧热影响区硬度出现了硬化, K418 侧热影响区硬度略低于母材。42CrMo 侧热影响区硬化是由于在 42CrMo 侧热影响区出现了针状马氏体, 如图 7 所示。焊缝区域硬度低于 K418 母材, 这是由于 K418 的主要强化相是 γ' , 激光焊接的快速凝固可以抑制焊缝区域的 γ' 产生, 使焊缝区域的 γ' 数量减少^[8]。焊缝区通过扫描电镜观察到热裂纹, 如图 8 所示。对焊缝区域 1 和裂纹处区域 2 能谱分析表明裂纹处 Mo, Al, Nd, Ti 元素聚集, 如表 3 和图 8 所示, 这些元素的聚集易在焊缝中形成 Laves, $\gamma + \gamma'$ 共晶及其它的低熔物, 在焊接应力作用下极易成为裂纹萌生和扩展的地方^[9, 10]。在金相显微镜下观察到焊缝与 K418 交界呈锯齿形, 如图 9 所示, 这是由于 K418 熔化金属的流动性差, 导致焊缝靠近 K418 侧熔池金属对流传热不充分。

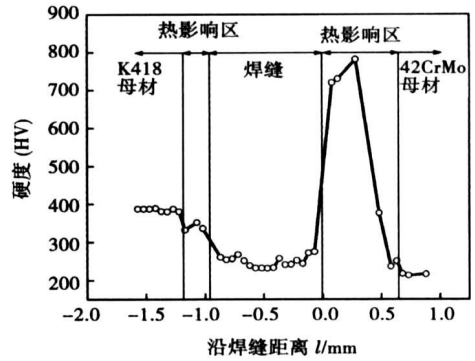


图 6 沿焊缝横截面的硬度分布

Fig. 6 Hardness as function of distance from joint interface

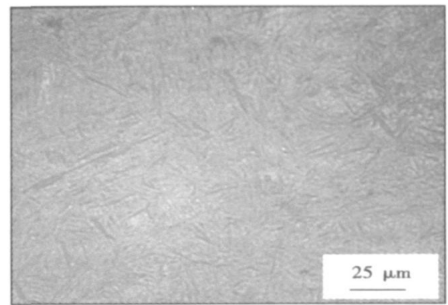


图 7 42CrMo 侧热影响区

Fig. 7 Heat affected zone of 42CrMo

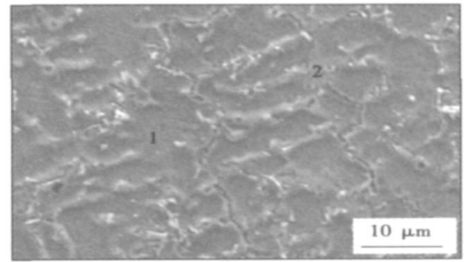


图 8 焊缝区域裂纹

Fig. 8 Weld region crack

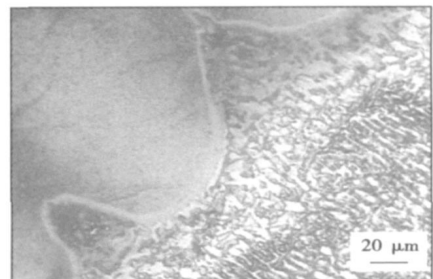


图 9 焊缝与 K418 交界

Fig. 9 Interface between weld and K418

表 3 焊缝区域成分分析(质量分数, %)
Table 3 EDS analysis results of laser weld

	Ni	Fe	Cr	Mo	Al	Nb	Ti	Mn
区域 1	54.268 6	32.026 0	7.644 3	1.890 7	0.826 0	2.322 8	0.882 0	0.139 7
区域 2	37.926 9	27.939 3	8.753 2	6.0603	1.857 7	12.959	4.503 5	0

4 结 论

(1) K418 与 42CrMo 异种金属激光深熔焊接, 宜采用激光光斑偏向 42CrMo 侧, 以克服它们的物理化学性质的差异导致焊缝靠进 42CrMo 侧出现的未熔合。

(2) 随激光焊接速度的减少和激光功率的增加, 激光作用在焊缝处的能量升高, 焊缝熔深增加。

(3) 通过优化侧吹保护气流量可以增加焊缝熔深。

(4) 激光焊接厚板 K418 和 42CrMo 异种金属, 为了获得较大熔深, 宜利用激光光束的传输特性, 采用接近瑞利长度范围内的负离焦。

(5) 焊缝区热裂纹的产生主要是由于焊缝区元素的偏析在晶界形成的低熔物导致。

参考文献:

[1] Lee J W. Inertia friction welding of a gas turbine rotor[J]. *Welding Review International*, 1992, 11(4): 189-192.

[上接第 82 页]

[8] 彭云, 王成, 陈武柱, 等. 两种规格超细晶粒钢的激光焊接[J]. *焊接学报*, 2001, 22(1): 31-35.

[9] Zhang Xudong, Chen Wuzhu, Wang Cheng *et al.* Microstructures and toughness of weld metal of ultra-fine grained ferritic steel by laser welding[J]. *Journal of Materials Science & Technology*, 2004, 20(6): 755-759.

[10] 赵琳, 陈武柱, 张旭东. 新一代超低碳贝氏体钢激光焊接热影响区的组织和性能[J]. *中国激光*, 2006, 33(3): 408-412.

[11] Chornamoryan S A, Chemyshova T A, Blinov V M, *et al.* Hot

[2] 杜随更, 傅莉, 曹营, 等. K418 涡轮盘和 42CrMo 轴摩擦焊接头的强化[J]. *西北工业大学学报*, 2004, 22(1): 112-115.

[3] 吕百达. 激光光学—激光束的传输变换和光束质量控制[M]. 重庆: 四川大学出版社, 1992.

[4] 工程材料实用手册编辑委员会. 工程材料实用手册(2)[M]. 北京: 中国标准出版社, 1989.

[5] 谭真, 郭广文. 工程合金热物性[M]. 北京: 冶金工业出版社, 1994.

[6] 虞钢, 虞和济. 集成化激光智能加工工程[M]. 北京: 冶金工业出版社, 2001.

[7] 庞铭, 虞钢, 刘兆, 等. K418 与 42CrMo 异种金属的激光穿透焊接[J]. *中国激光*, 2006, 33(8): 1122-1126.

[8] Sekhar N C, Read R C. Power beam welding of thick section nickel base superalloys[J]. *Science and Technology of Welding and Joining*, 2002, 7(2): 77-86.

[9] Radhakrishna Ch, Prasad Rao K. The formation and control of laves phase in superalloy 718 welds[J]. *Journal of Materials Science*, 1997, 32: 1977-1984.

[10] 冯钟潮, 于尔靖, 朱鸿德, 等. 铸造镍基合金液化裂纹[J]. *焊接学报*, 1983, 4(2): 79-86.

作者简介: 庞铭, 男, 1980 年出生, 博士研究生。主要从事激光焊接试验与数值模拟研究。发表论文 3 篇。

Email: pangming@imech.ac.cn

cracking when welding high-nitrogen austenitic steels[J]. *Welding International*, 1993, 7(9): 730-733.

[12] Nishimoto K, Mori H. Hot cracking susceptibility in laser weld metal of high nitrogen stainless steels[J]. *Science and Technology of Advanced Materials*, 2004, 5(1-2): 231-240.

作者简介: 赵琳, 男, 1977 年出生, 工学博士。主要从事材料焊接性、激光材料加工等方面的科研工作。发表论文 20 余篇。

Email: lhnds@yahoo.com.cn

Key words: servoguns; single sided spot welding; shear strength; welding deformation

Foundation of steady state creep constitutive equation of SnCu soldered joints

YAN Yanfu¹, JI Lianqing², ZHANG Keke¹, YAN Hongxin¹, FENG Lifang¹ (1. School of Materials Science and Engineering, Henan University of Science and Technology, Luoyang 471003, Henan, China; 2. School of Mechatronics Engineering, Zhengzhou University of Light Industry, Zhengzhou 450002, China). p75—79

Abstract: SnCu eutectic solder alloys have been regarded as one of the most promising Pb-free substitutes for the SnPb solders for its low cost and good mechanical properties. Creep property of solder alloys is one of the important factors to affect the reliability of soldered joints. A novel high temperature creep strain equipment was used to test stress exponent and creep activation energy of single shear lap creep specimens of SnCu eutectic soldered joints with a 1 mm² cross-sectional area. The final constitutive equation of the composite soldered joints was established and its creep mechanism was investigated. Results indicate under low temperature and high stress, the stress exponents of the soldered joints is 8.73, and the creep activation energies is varied in 59.1—63.2 kJ/mol. The dislocation climbing is dominated by dislocation pipe diffusion process. Under high temperature and low stress, the stress exponents of the soldered joints is 6.45 and the creep activation energies is varied from 88.4—97.5 kJ/mol. The dislocation climbing is dominated by the lattice self-diffusion process.

Key words: SnCu solder; stress exponent; activation energy; steady-state creep constitutive equation; creep mechanism

Laser welding of high nitrogen steel 1Cr22Mn16N—II. microstructure and mechanical properties of weld metal

ZHAO Lin^{1,2}, TIAN Zhiling¹, PENG Yun^{1,2}, ZHAO Xiaobing^{1,2}, QI Yanchang^{1,2} (1. State Key Laboratory of Advanced Steel Processes and Products, Central Iron & Steel Research Institute, Beijing 100081, China; 2. Division of Structural Materials, Central Iron & Steel Research Institute, Beijing 100081, China). p80—82, 86

Abstract: In order to study the microstructure and mechanical properties of the weld metal of high nitrogen steel 1Cr22Mn16N, the steel was welded by CO₂ laser welding, and the influence of the shielding gas composition and heat input on the microstructure and mechanical properties of the weld metal was investigated. The experimental results indicate that the microstructure in the weld metal is austenite and δ -ferrite. The size of δ -ferrite is increased with the increase of heat input. The results also show that no soft zone occurs in the weld metal. The hardness of weld metal is increased as the heat input is decreased, and it is improved as N₂ in the shielding gas is increased. The toughness increases when the heat input decreases, whereas the compositions of shielding gas probably have no influence on the change of toughness of the weld metal.

Key words: high nitrogen steel; laser welding; weld metal; microstructure; mechanical properties

Deep penetration laser welding dissimilar metal of K418 and 42CrMo

PANG Ming, ZHENG Caiyun, LIU Xiubo, YU Gang (Institute of Mechanics, Chinese Academy of Sciences, Beijing 100080, China). p83—86

Abstract: The influences of laser power, welding velocity, defocusing distance and flow rate of side-blow shielding gas on shape of weld, and weld penetration of laser deep penetration welding of dissimilar metal K418 and 42CrMo were experimentally investigated using continuous wave (CW) Nd:YAG laser. Mechanism of hot crack formation of weld zone was analyzed. Results show that lack fusion between weld and 42CrMo interface is observed due to difference of their physical and chemical properties. Offset of laser beam toward 42CrMo can abate lack fusion between weld and 42CrMo interface. The serrate shape is observed between weld seam and K418 interface due to not full convection heat transfer. Weld penetration can be increased by optimization flow rate of side-flow shielding gas and defocusing distance. The main cause of hot crack in the weld zone of dissimilar metal of K418 and 42CrMo laser welding is the segregation of the element and the forming of low-melting phases over grain boundaries.

Key words: laser welding; deep penetration welding; weld; hot cracks

Vacuum brazing of SiC_p/Cu composite

ZHANG Jie, XU Xiaojing, DAI Fengze (Mechanical Engineering Department, Jiangsu University, Zhenjiang 212013, Jiangsu, China). p87—90

Abstract: Vacuum brazing of SiC_p/Cu composite fabricated by powder metallurgy and followed by hot extrusion was carried out with Ti and AgCuTi brazing filler metal in different condition. The morphologies of joint shear fracture and shear strength were also investigated by means of scanning electron microscope and shearing test. The results showed that the bonding of SiC_p/Cu composite performed with Ti filler is better than that with AgCuTi. The maximum shear strength of the joint brazed at 850 °C for 20 min is up to 70.5 MPa. When the volume fraction of SiC_p increases, the shear strength of the joint decreases, and when the volume fraction of SiC_p is more than 10 vol.%, the shear strength of the joint decreases more quickly.

Key words: SiC_p/Cu composite; vacuum brazing; bonding strength

Forming conditions of Fe—Ni—Si—B amorphous coating by laser cladding

ZHU Qingjun, ZOU Zengda, WANG Xinhong, QU Shiyao (School of Materials Science and Engineering, Shandong University, Jinan 250061, China). p91—94

Abstract: A Fe—Ni—Si—B amorphous coatings was prepared by laser cladding on the substrate 45 carbon steel with a 5 kW continuous CO₂ laser. The phases, microstructure and the forming